

LETTER TO THE EDITOR

## Strongly correlated wave functions for artificial atoms and molecules

**Constantine Yannouleas and Uzi Landman**

School of Physics, Georgia Institute of Technology, Atlanta, Georgia 30332-0430

**Abstract.** A method for constructing semianalytical strongly correlated wave functions for single and molecular quantum dots is presented. It employs a two-step approach of symmetry breaking at the Hartree-Fock level and of subsequent restoration of total spin and angular momentum symmetries via Projection Techniques. Illustrative applications are presented for the case of a two-electron helium-like single quantum dot and a hydrogen-like quantum dot molecule.

Published: J. Phys.: Condens. Matter **14**, L591 (2002)

PACS numbers: 73.21.La, 71.27.+a

Understanding the nature of strong many-body correlations in condensed-matter finite systems is a fundamental task, which can be facilitated by devising analytical or semi-analytical many-body wave functions that approximate well the exact solutions and capture the essential physical properties of such systems. The description of strong correlations in the two-dimensional (2D) electron gas in a high magnetic field by the Laughlin wave function [1] represents a celebrated example of such a methodology.

Here we construct semianalytical correlated wave functions for electrons in 2D single and molecular Quantum Dots (QD's), which are manmade devices created at semiconductor interfaces and are most often referred to as artificial atoms and molecules (since they contain a finite number of electrons). To this end, we employ a two-step approach consisting of symmetry breaking at the Hartree-Fock single-determinantal level and subsequent symmetry restoration via Projection Techniques (PT's) resulting in multi-determinantal wave functions. PT's have been introduced earlier in Quantum Chemistry [2] for the restoration of the total spin of a molecule and in Nuclear Physics [3, 4] for the restoration of the total 3D angular momentum (space rotational symmetry) of deformed open-shell nuclei. Our application of these methods to circular single quantum dots (SQD's) requires the simultaneous restoration of both the spin and the angular-momentum symmetries. This requirement poses a more demanding challenge compared to the task of restoring a single broken symmetry, as is the case with the Quantum-Chemistry and Nuclear-Physics many-body problems.

Since the approach of restoration of broken symmetries is largely untested and unknown in the framework of 2D QD's, we aim in this paper at focusing on methodological aspects. For simplicity and conceptual clarity, we construct below strongly correlated wave functions for the case of two interacting electrons in a SQD (artificial helium, He-QD) and in a lateral double quantum dot (artificial hydrogen quantum dot molecule, H<sub>2</sub>-QDM). Two strongly-correlated electrons (with or without an external magnetic field) may exhibit a complex behavior [1, 5, 6] and can provide the foundation for understanding the properties of a larger number of interacting electrons. Furthermore, the recent growth of interest in quantum computing focussed attention on the potential ability to manipulate the ground-state entanglement of two-electron quantum-dot systems [7].

The two-body hamiltonian for two interacting electrons constrained to move on a plane is given by,

$$\mathcal{H} = H(\mathbf{r}_1) + H(\mathbf{r}_2) + e^2/\kappa r_{12} , \quad (1)$$

where the last term is the Coulomb repulsion with  $\kappa$  being the dielectric constant of the semiconductor material.  $H(\mathbf{r})$  is the single-particle hamiltonian for an electron in an external perpendicular magnetic field  $\mathbf{B}$  and an appropriate potential confinement. For a QDM, the external confinement is given by a two-center-oscillator potential, and the single-particle hamiltonian is written as,

$$H = T + \frac{1}{2}m^*\omega_0^2(x^2 + y_k'^2) + V_{\text{neck}}(y) + \frac{g^*\mu_B}{\hbar}\mathbf{B} \cdot \mathbf{s} , \quad (2)$$

where  $y_k' = y - y_k$  with  $k = 1$  for  $y < 0$  (left) and  $k = 2$  for  $y > 0$  (right).  $x$  denotes the coordinate perpendicular to the interdot axis ( $y$ ).  $T = (\mathbf{p} - e\mathbf{A}/c)^2/2m^*$ , with  $\mathbf{A} = 0.5(-By, Bx, 0)$ , and the last term in Eq. (2) is the Zeeman interaction with  $g^*$  being the effective  $g$  factor,  $\mu_B$  the Bohr magneton, and  $\mathbf{s}$  the spin of an individual electron. The shapes described by  $H$  are two equal semi-circles connected by a smooth neck  $[V_{\text{neck}}(y)]$ .  $-y_1 = y_2 > 0$  are the centers of these semi-circles,  $d = y_2 - y_1$  is the interdot distance, and  $m^*$  is the effective electron mass. The case

of a SQD is obtained for  $d = 0$ , and in this case the confining potential is purely parabolic. For the smooth neck, we use  $V_{\text{neck}}(y) = \frac{1}{2}m^*\omega_0^2[C_k y_k'^3 + D_k y_k'^4]\theta(|y| - |y_k|)$ , where  $\theta(u) = 0$  for  $u > 0$  and  $\theta(u) = 1$  for  $u < 0$ . The constants  $C_k$  and  $D_k$  can be expressed via one parameter, as follows:  $C_k = (2 - 4\epsilon^b)/y_k$  and  $D_k = (1 - 3\epsilon^b)/y_k^2$ , where the barrier-control parameter  $\epsilon^b = V_b/V_0$  is related to the actual (controlable) height of the bare barrier ( $V_b$ ) between the two QD's, and  $V_0 = m^*\omega_0^2 y_1^2/2$ . The single-particle levels of  $H$  are obtained by numerical diagonalization (for details see Ref. [10]).

In each case, in the first step of our procedure, the two-electron hamiltonian [Eq. (1)] is solved [8, 9, 10] in the (symmetry-breaking) spin-and-space unrestricted Hartree-Fock (sS-UHF) approximation; for comparison, the symmetry-adapted restricted Hartree-Fock (RHF) will also be considered. In all cases, we will use  $\hbar\omega_0 = 5$  meV and  $m^* = 0.067m_e$  (this effective-mass value corresponds to GaAs). We will vary the dielectric constant  $\kappa$ , however, in order to control the ratio of the strength of the Coulomb repulsion relative to the zero-point kinetic energy (see in particular the case of the SQD and figure 3 below). The variation of this ratio provides us with the ability to study the whole range of electron correlations, from the regime of weak correlations to that of strong correlations.

We start with the case of a lateral H<sub>2</sub>-QDM in a magnetic field, where only the spin projection needs to be considered, since the confining potential lacks circular symmetry. The example we discuss here<sup>‡</sup> corresponds to the case of weak interelectron repulsion (the full choice of parameters is given in the caption of Fig. 1). The sS-UHF determinant (henceforth we drop the prefix sS in subscripts) which describes the “singlet” (see below) ground state of the H<sub>2</sub>-QDM is given by the expression,

$$|\Phi_{\text{UHF}}(1, 2)\rangle = |u(1)\bar{v}(2)\rangle/\sqrt{2}. \quad (3)$$

In Eq. (3), we have used a compact notation for the Slater determinant with  $u(1) \equiv u(\mathbf{r}_1)\alpha(1)$  and  $\bar{v}(2) \equiv v(\mathbf{r}_2)\beta(2)$ , where  $u(\mathbf{r})$  and  $v(\mathbf{r})$  are the 1s-like (left) and 1s'-like (right) localized orbitals of the sS-UHF solution, and  $\alpha$  and  $\beta$  denote the up and down spin functions, respectively. Such orbitals for the field-free case are displayed in Fig. 1(a) (left column). Similar localized orbitals (which are complex functions) can appear also in the  $B \neq 0$  case [see Fig. 1(b), right column].

$|\Phi_{\text{UHF}}(1, 2)\rangle$  is an eigenstate of the  $z$ -projection of the total spin,  $\hat{\mathbf{S}} = \hat{\mathbf{s}}_1 + \hat{\mathbf{s}}_2$ , with eigenvalue  $S_z = 0$ . However, it is not an eigenstate of the square,  $\hat{\mathbf{S}}^2$ , of the total spin (thus the quotation marks in “singlet” above). From the determinant  $|\Phi_{\text{UHF}}(1, 2)\rangle$ , one can generate a singlet eigenstate of  $\hat{\mathbf{S}}^2$  (with zero eigenvalue) by applying the projection operator  $P_0 \equiv 1 - \varpi_{12}$ , where the operator  $\varpi_{12}$  interchanges the spins of the two electrons.

Thus the singlet state of the two localized electrons is given by the projected wave function,

$$|\Psi(1, 2)\rangle \equiv P_0|\Phi_{\text{UHF}}(1, 2)\rangle \propto |u(1)\bar{v}(2)\rangle - |\bar{u}(1)v(2)\rangle. \quad (4)$$

In contrast to the single-determinantal wave functions of the RHF and sS-UHF methods, the projected many-body wave function (4) is a linear superposition of two Slater determinants, and thus it is an entangled state representing a corrective (post-Hartree-Fock) step beyond the mean-field approximation. We notice that the spatial reflection symmetry is automatically restored along with the spin symmetry.

<sup>‡</sup> For a systematic study of the H<sub>2</sub>-QDM at different values of  $\kappa$  [including  $\kappa = 12.9$  (GaAs)] and interdot barrier heights, demonstrating gate control of the entanglement of a pair of electrons, see Ref. [10].

Eq. (4) has the form of a Heitler-London (HL) or valence bond [11] wave function. However, unlike the original HL scheme which uses the orbitals  $\phi_L(\mathbf{r})$  and  $\phi_R(\mathbf{r})$  of the separated (left and right) QD's, expression (4) employs the sS-UHF orbitals which are self-consistently optimized for any separation  $d$ , interdot barrier height  $V_b$ , and magnetic field  $B$ . Consequently, expression (4) can be characterized as a Generalized Heitler-London (GHL) wave function. In the context of QD's, the simple HL approach has been proven very useful in demonstrating [7] that the H<sub>2</sub>-QDM under an external magnetic field can function as an elemental two-qubit logic gate. Our more accurate GHL approach has the potential of greatly improving the quality of similar investigations regarding the implementation of quantum computing using solid-state nanodevices.

We further notice that our GHL method belongs to a class of projection techniques known as variation before projection (VBP), unlike the familiar in Quantum Chemistry Generalized Valence Bond method [12], or the Spin-Coupled Valence Bond method [13], which employ a variation after projection (VAP) (see e.g. ch. 11.4.2 of Ref. [4]). In the context of QD's, a generalization of our GHL approach along the VAP technique may provide even more accurate results. This, however, is left for future work, including the development of the pertinent computer codes.

The energy of a projected state is given [4] in general by the formula,

$$E_{\text{PROJ}} = \langle \Phi_{\text{UHF}} | \mathcal{H} \mathcal{O} | \Phi_{\text{UHF}} \rangle / \langle \Phi_{\text{UHF}} | \mathcal{O} | \Phi_{\text{UHF}} \rangle , \quad (5)$$

where  $\mathcal{H}$  is the many-body hamiltonian and  $\mathcal{O}$  is a general projection operator with the property  $\mathcal{O}^2 = \mathcal{O}$ .

Using the spin-projection operator  $P_0$  in place of  $\mathcal{O}$ , we find for the total energy,  $E_{\text{GHL}}^s$ , of the singlet GHL state,

$$E_{\text{GHL}}^s = \mathcal{N}_s^2 [H_{uu} + H_{vv} + S_{uv}H_{vu} + S_{vu}H_{uv} + J_{uv} + K_{uv}] , \quad (6)$$

where  $H_{uu}$ , etc., are the matrix elements of the single-particle hamiltonian  $H$  in Eq. (1), and  $J$  and  $K$  are the direct and exchange matrix elements of  $e^2/\kappa r_{12}$ .  $S_{uv}$  is the overlap integral of the  $u(\mathbf{r})$  and  $v(\mathbf{r})$  orbitals,

$$S_{uv} = \int u^*(\mathbf{r})v(\mathbf{r})d\mathbf{r} , \quad (7)$$

and the normalization parameter is given by

$$\mathcal{N}_s^2 = 1/(1 + S_{uv}S_{vu}) . \quad (8)$$

At zero magnetic field, the electron orbitals are real functions and Eqs. (6) – (8) reduce to a form familiar from the Generalized Valence Bond theory of Quantum Chemistry [12].

For the triplet state with  $S_z = \pm 1$ , the projected wave function coincides with the original HF determinant, so that the corresponding energies in all three approximation levels are equal, i.e.,  $E_{\text{GHL}}^t = E_{\text{RHF}}^t = E_{\text{UHF}}^t$ .

In Fig. 1(c), we display the singlet-triplet energy gap,  $\Delta\varepsilon = E^s - E^t$ , of the H<sub>2</sub>-QDM as a function of the magnetic field  $B$ . For all three levels of approximation,  $\Delta\varepsilon$  starts from a negative minimum (singlet ground state) and after crossing the zero value it remains positive (triplet ground state). However, after crossing the zero line, the RHF curve incorrectly continues to rise sharply and moves outside of the plotted range. After reaching a broad maximum, the positive  $\Delta\varepsilon$  branches of both the sS-UHF and GHL curves approach zero for sufficiently large  $B$ , a behavior which indicates that the H<sub>2</sub>-QDM dissociates with  $B$ . This molecular dissociation can be further seen in

**FIGURE 1**  
**SEPARATE GIF**

**Figure 1.** H<sub>2</sub>-QDM: The two occupied orbitals (modulus square) of the symmetry broken “singlet” sS-UHF solution for (a)  $B = 0$  and (b)  $B = 9$  T. (c) The singlet-triplet energy difference as a function of an external perpendicular magnetic field and for three successive levels of approximation, i.e., the RHF (top solid curve), the sS-UHF (dashed curve), and the GHL (bottom solid curve). The choice of parameters is: parabolic confinement of each dot  $\hbar\omega_0 = 5$  meV, interdot distance  $d = 30$  nm, interdot barrier height  $V_b = 3.71$  meV, effective mass  $m^* = 0.067m_e$ , and dielectric constant  $\kappa = 45$ . The effective Zeeman coefficient was chosen  $g^* = 0$ ; for a small nonvanishing value, like  $g^* = -0.44$ , the Zeemann splitting does not alter the orbital densities and can be simply added to  $\Delta\varepsilon$ . Up and down arrows denote spins. Distances are in nm and the densities in  $10^{-4}$  nm<sup>-2</sup>.

the orbitals themselves: at  $B = 9$  T [Fig. 1(b)] the orbitals are well localized on the individual dots, while at  $B = 0$  [Fig. 1(a)] they extend over the entire QDM. Note that, in addition to having the proper symmetry, GHL is energetically the best approximation.

We further note that systematic explorations for determining the border of HF instability (i.e., the appearance of broken symmetry solutions with lower energy) in the case of the H<sub>2</sub>-QDM are not available. At  $B = 0$ , this border depends on all four parameters  $\hbar\omega_0$ ,  $\kappa$ ,  $d$ , and  $V_b$ . For  $\hbar\omega_0 = 5$  meV,  $d = 30$  nm, and  $\kappa = 45$ , it was found [10] that this border can be crossed by reducing the interdot barrier  $V_b$  to zero. For the same values of  $B$ ,  $\hbar\omega_0$  and  $d$ , but for a different  $\kappa = 12.9$  (stronger interelectron repulsion, as is the case for GaAs), however, all values of the interdot barrier ( $V_b \geq 0$ ) represent cases that lie well within the region of instability.

Next we address the case of two electrons at  $B=0$  in a single QD with a parabolic confinement. As we have shown in earlier publications [8, 9], the sS-UHF solution does not preserve the rotational symmetry for  $R_W \geq 1.0$  (for  $R_W < 1.0$ , the sS-UHF solution collapses onto the RHF one). The Wigner parameter  $R_W$  expresses the ratio between the interelectron repulsion  $Q$  and the zero-point kinetic energy  $K$ ; it is customary to take  $Q = e^2/\kappa l_0$  and  $K \equiv \hbar\omega_0$ , where  $l_0 = (\hbar/m^*\omega_0)^{1/2}$  is

the spatial extent of an electron in the lowest state of the parabolic confinement. This gives  $R_W \propto 1/(\kappa\sqrt{\omega_0})$ , showing that it can be varied through the choice of materials (i.e.,  $\kappa$ ) and/or the strength of the confinement ( $\omega_0$ ). For  $R_W \geq 1.0$  and for  $S_z = 0$ , the sS-UHF yields [9] an infinite manifold of azimuthally degenerate ground-state configurations consisting of two localized antipodal orbitals, suggesting formation of an electron molecule [6, 8, 9] (also referred to as Wigner molecule). For  $\kappa = 8$  ( $R_W = 2.39$ ) and for a specific azimuthal direction (i.e.,  $\gamma = 0$ ), the two localized orbitals,  $u(\mathbf{r})$  and  $v(\mathbf{r})$  with up and down spin, respectively, are depicted in Fig. 2(a). As was the case with the double-dot example studied above, the  $S_z = 0$  sS-UHF determinant  $|\Phi_{\text{UHF}}(1, 2)\rangle$  for  $\gamma = 0$  is given by Eq. (3) and thus, in addition to the rotational symmetry, it does not preserve the total-spin symmetry. For the singlet state, one can restore both symmetries successively, namely, one can generate appropriate projected wave functions,

$$|\Psi_I(1, 2)\rangle \equiv \mathcal{O}|\Phi_{\text{UHF}}(1, 2)\rangle, \quad (9a)$$

by applying the product operator,§

$$\mathcal{O} \equiv \mathcal{P}_I P_0, \quad (9b)$$

where the spin-projection operator  $P_0$  produces a two-determinant singlet GHL wave function as previously explained. The angular-momentum projection operator  $\mathcal{P}_I$  yields multideterminantal wave functions having good total angular momentum  $I$ . This latter operator produces a linear superposition of an infinite number of azimuthal GHL wave functions and it is given|| by [4],

$$2\pi\mathcal{P}_I \equiv \int_0^{2\pi} d\gamma \exp[-i\gamma(\hat{L} - I)], \quad (10)$$

where  $\hat{L} = \hat{l}_1 + \hat{l}_2$  is the operator for the total angular momentum. In the following we focus on the ground state¶ of the system with  $I = 0$ .

It is instructive to examine the transformations of the ground-state electron densities (ED's) resulting from the successive approximations, RHF, sS-UHF, spin projection (SP), and combined spin and angular momentum projection (S&AMP). For  $\kappa = 8$ , such ED's are shown in Fig. 2. Since the exact solution for two electrons in a parabolic confinement is available [6], we also plot the corresponding ED for the exact ground state in Fig. 2(f). The ED's of the initial RHF [Fig. 2(b)] and the final S&AMP [Fig. 2(e)] approximations are circularly symmetric, while those of the two intermediate approximations, i.e., the sS-UHF and SP, do break the circular symmetry. This behavior graphically illustrates the meaning of the term restoration of symmetry and the interpretation that the sS-UHF broken-symmetry solution refers to the *intrinsic* (rotating) frame of reference of the electron molecule. We notice that the S&AMP electron density exhibits a characteristic flattening at the top in contrast to the more Gaussian-type RHF one. Thus, although not identical (the exact ED is slightly flatter at the top), the S&AMP ED closely resembles the exact one displayed in Fig. 2(f). Further, we remark that the SP electron density exhibits in the middle

§ In the case of a triplet state, the sS-UHF determinant with  $S_z = \pm 1$  preserves the total spin, and thus the application of  $\mathcal{P}_I$  alone is sufficient.

|| The corresponding expression [3] for the 3D angular-momentum projection uses the Wigner functions  $\mathcal{D}_{MK}^I(\Omega)$  (see also ch. 11.4.6 in Ref. [4]).

¶ The family of projected wave functions (9) describes all the lowest-energy (yrast band [6]) states with good angular momentum  $I = 2, 4, \dots$ , in addition to the ground state ( $I = 0$ ). The yrast-band states with odd values,  $I = 1, 3, 5, \dots$ , are generated via a projection of the triplet state.

**FIGURE 2  
SEPARATE GIF**

**Figure 2.** He-QD at  $B = 0$ : (a) The two occupied orbitals (modulus square) of the symmetry-broken “singlet” sS-UHF solution. The rest of the frames display the electron densities at successive approximation levels, i.e., (b) RHF, (c) sS-UHF, (d) SP alone, (e) S&AMP, and (f) exact. See the text for a description of the acronyms. The choice of parameters is: dielectric constant  $\kappa = 8$ , parabolic confinement  $\hbar\omega_0 = 5$  meV, and effective mass  $m^* = 0.067m_e$ . Distances are in nm and the densities in  $10^{-4}$  nm $^{-2}$ .

a shallower depression than the corresponding sS-UHF one, in keeping with the fact that the covalent bonding increases the probability of finding the electrons between the individual dots.

Using the projection operator (9b) in the general Eq. (5), we obtain for the energy  $E_{\text{S\&AMP}}$  of the fully projected ground state of the two-electron single QD,

$$E_{\text{S\&AMP}} = \int_0^{2\pi} h(\gamma) d\gamma / \int_0^{2\pi} n(\gamma) d\gamma , \quad (11)$$

with

$$h(\gamma) = H_{us}S_{vt} + H_{ut}S_{vs} + H_{vt}S_{us} + H_{vs}S_{ut} + V_{uvst} + V_{uvts} , \quad (12)$$

and

$$n(\gamma) = S_{us}S_{vt} + S_{ut}S_{vs} , \quad (13)$$

$s(\mathbf{r})$  and  $t(\mathbf{r})$  being the  $u(\mathbf{r})$  and  $v(\mathbf{r})$  sS-UHF orbitals rotated by an angle  $\gamma$ , respectively.  $V_{uvst}$  and  $V_{uvts}$  are two-body matrix elements of the Coulomb repulsion.<sup>+</sup> Observe that  $E_{\text{S\&AMP}}$  represents a rotational average over all the possible orientations of the electron molecule and that  $h(0)/n(0)$  coincides with the expression (6) for the energy  $E_{\text{GHL}}^s$  of the covalently bonded H<sub>2</sub>-QDM.

<sup>+</sup>  $V_{uvst} \equiv (e^2/\kappa) \int d\mathbf{r}_1 \int d\mathbf{r}_2 u^*(\mathbf{r}_1)v^*(\mathbf{r}_2)(1/r_{12})s(\mathbf{r}_1)t(\mathbf{r}_2)$ . In Eq. (6)  $J_{uv} = V_{uvuv}$  and  $K_{uv} = V_{uvvu}$ .

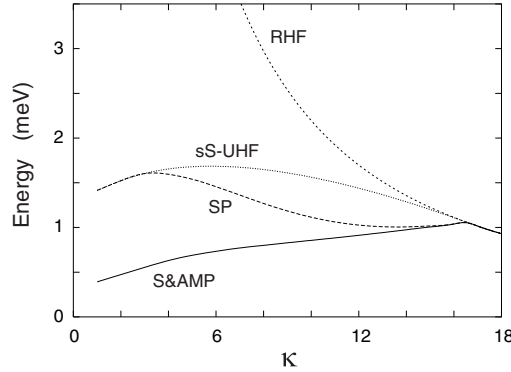


**Figure 3.** He-QD at  $B = 0$ : Difference between the ground-state energies of various approximations and the exact one, plotted vs. the dielectric constant  $\kappa$ . From top to bottom, the curves correspond to the RHF, the sS-UHF, the SP alone, and the combined S&AMP approximation. The curve labeled RHF gives the correlation energy. The choice of parameters is: parabolic confinement  $\hbar\omega_0 = 5$  meV, and effective mass  $m^* = 0.067m_e$ .

To further examine how closely expression (9) describes the ground state of the He-QD, we display in Fig. 3 the energy deviations of the four approximation steps (i.e., RHF, sS-UHF, SP, and S&AMP) from the exact (EX) [6] ground state, as a function of the dielectric constant  $\kappa$ . The variation of  $\kappa$  produces a variation in the strength of the interelectron repulsion, with a larger repulsion (i.e., smaller  $\kappa$ ) corresponding to stronger electron correlations.

The correlation energy,  $E_{\text{cor}} \equiv E_{\text{RHF}} - E_{\text{EX}}$ , is defined as the difference between the RHF ground-state energy and the exact one, and thus it coincides with the top curve in Fig. 3 denoted as RHF. The ordering (from top to bottom) of the curves in Fig. 3 reflects the fact that each subsequent approximation step captures successively a larger portion of the total correlations, and thus lowers the total energy. From Fig. 3, one sees that there are two correlation regimes: In the regime of weak correlations, the three lower curves collapse onto the RHF one; naturally, this regime corresponds to the normal Fermi liquid and extends to  $\kappa \rightarrow \infty$ . The onset of strong correlations and of symmetry-broken HF solutions occurs at  $\kappa = 16.5$  ( $R_W = 1.16$ ) and extends to  $\kappa = 0$ .

Note that the percentage,  $E_{\text{cor}}/E_{\text{EX}}$ , of correlations with respect to the exact energy is 6.8% and 49.5% for  $\kappa = 16.50$  and  $\kappa = 1$ , respectively. These values are much higher than the values encountered in natural atoms; for this reason, 2D QD's are referred to as strongly correlated systems. Thus it is not surprising that the RHF error in Fig. 3 grows exponentially for stronger correlations (smaller  $\kappa$  or larger  $R_W$ ). However, it is remarkable that the S&AMP approximation (where all symmetries have been restored) converges to the exact result for smaller  $\kappa$ . Note that the exact ground-state energy is 19.80 meV for  $\kappa = 8$  ( $R_W = 2.39$ ) and 51.83 meV for  $\kappa = 1$  ( $R_W = 19.09$ ), resulting for the S&AMP in a relative error of 4% and 0.7%, respectively.\* These results are in agreement with the experience from Nuclear Physics, where it has been found [4] that the VBP yields reliable results in the case

\* For  $\kappa = 8$ , the fraction of correlation energy captured by the successive approximations is: sS-UHF 44.4%, SP 57.2%, and S&AMP 73.1%; the corresponding values for  $\kappa = 1$  are: 94.5%, 94.5%, and 98.5%.



of strong symmetry breaking (strongly deformed nuclei).

Interestingly, the SP curve collapses onto the sS-UHF one for  $\kappa \leq 3.2$ . This behavior defines [8] an intermediate regime $\ddagger$  between the Fermi-liquid and the regime of strongly crystallized Wigner molecules ( $\kappa \leq 3.2$ ). In the latter regime, the overlap ( $S_{uv}$ ) between the antipodally localized electron orbitals is very small, such that the sS-UHF energy is not effectively lowered by the spin projection (SP).

We have demonstrated that the sS-UHF method in conjunction with the companion step of restoration of the spin and space symmetries via Projection Techniques (when such symmetries are broken) can provide appropriate semianalytical wave functions for an accurate description of strongly correlated electrons in artificial atoms and molecules.

This research is supported by the US D.O.E. (Grant No. FG05-86ER-45234).

## References

- [1] Laughlin R B 1983 *Phys. Rev. Lett.* **50** 1395; 1983 *Phys. Rev. B* **27** 3383
- [2] Löwdin P O 1955 *Phys. Rev. B* **97** 1509; 1964 *Rev. Mod. Phys.* **36** 966
- [3] Peierls R E and Yoccoz J 1957 *Proc. Phys. Soc., London, Sect. A* **70** 381
- [4] Ring P and Schuck P *The Nuclear Many-body Problem* (Springer, New York, 1980) ch. 11.4.4.
- [5] Merkt U et al 1991 *Phys. Rev. B* **43** 7320
- [6] Yannouleas C and Landman U 2000 *Phys. Rev. Lett.* **85** 1726
- [7] Burkard G et al 1999 *Phys. Rev. B* **59** 2070
- [8] Yannouleas C and Landman U 1999 *Phys. Rev. Lett.* **82** 5325; 2000 *Ibid.* **85** (E)2220
- [9] Yannouleas C and Landman U 2000 *Phys. Rev. B* **61** 15895
- [10] Yannouleas C and Landman U 2001 *ArXiv: cond-mat/0109167*
- [11] Heitler H and London F 1927 *Z. Phys.* **44** 455
- [12] Goddard III W A, Dunning, Jr. T H, Hunt W J and Hay P J 1973 *Acc. Chem. Res.* **6** 368
- [13] Gerratt J and Lipscomb W N 1968 *Proc. Natl. Acad. Sci. (USA)* **59** 332

$\ddagger$  In Ref. [8], we referred to the intermediate regime as the weak-Wigner-molecule regime. Such an intermediate regime may also arise in the infinite 2D electron gas at  $B = 0$ , see Pichard J-L et al *cond-mat/0107380*.

This figure "res\_jpcm\_fig1j.gif" is available in "gif" format from:

<http://arxiv.org/ps/cond-mat/0203571v2>

This figure "res\_jpcm\_fig2j.gif" is available in "gif" format from:

<http://arxiv.org/ps/cond-mat/0203571v2>